Impact of scalar mixing uncertainty on the predictions of reactor-based closures: application to a lifted methane/air jet flame

R. Amaduzzi[a,b*], A. Bertolino[a,b,c], A. Özden[a,b], R. Malpica Galassi[a,b], A. Parente[a,b*]

[a] *Aero-Thermo-Mechanics Laboratory, École Polytechnique de Bruxelles, Université Libre de Bruxelles, Belgium*

[b] *Brussels Institute for Thermal-fluid systems and clean Energy (BRITE), Université Libre de Bruxelles and Vrije Universiteit Brussel, Belgium*

[c] *Department of Chemistry, Materials, and Chemical Engineering "G. Natta", Politecnico di Milano, Milano 20133, Italy*

Abstract

This work is devoted to quantify the predictive uncertainty in RANS simulation of a non-premixed lifted flame due to uncertainty in the scalar dissipation rate transport equation model parameters. The uncertainty propagation and the global sensitivity analysis of the effect of such parameters on the quantities of interest (QoIs) is performed employing Polynomial Chaos Expansions as surrogate models of the uncertain response. This approach is applied on a lifted methane-air jet flame in vitiated coflow, already experimentally investigated by Cabra et al [1]. The results show the effectiveness of the approach to provide predictions with estimates of uncertainty. It is shown that the the uncertainty in the mixture fraction and temperature is negligible as long as only pure mixing happens, then it becomes significant in the regions where ignition begins, starting from $z/D = 30$. Of the four parameters considered C_{D1}, C_{D2}, C_{P1} and C_{P2}, main and total effect sensitivity indices shows that the largest contribution to the uncertainty in QoIs is given by the two dissipation parameters C_{D1} and C_{D2}, while the production parameter C_{P2} has almost negligible impact on the predictions. Lastly, the surrogate models are used to determine an optimum set of parameters that minimizes the distance with the experimental measures, leading to improved predictions of the QoIs.

Keywords: Uncertainty Quantification; Global sensitivity analysis; Partially Stirred Reactor; Polynomial Chaos Expansion; RANS;

1. Introduction

The world's ever growing demand for energy, combined with the commitment to reduce pollutants emissions, has led to the study and development of novel combustion technologies which can guarantee lower emissions and fuel flexibility, while the transition towards renewable energy sources unfolds. The combustion regimes that characterize such technologies often involve a diluted or vitiated coflow that strongly affects the behaviour of the reacting mixture. The ability of a combustion model to properly capture the turbulence/chemistry interactions is therefore essential to deliver predictive numerical simulations of novel combustion systems that are reliable on a quantitative level. Models that account for finite-rate chemistry proved to yield reasonable results [2–4] with respect to both temperature and species predictions. Among these, the Partially-Stirred Reactor (PaSR) closure model [5] was demonstrated to be suitable for combustion in vitiated conditions. Unlike other reactor-based models, in PaSR both mixing and chemical timescales are explicitly taken into account in the model formulation, allowing for a more detailed description of the interaction between turbulence and chemistry. It follows that the estimation of mixing and chemical timescales strongly affects the performance of the model.

For the estimation of chemical timescales different formulations already exist [5], usually based on formation or reaction rates of key species, which can be computed through the eigenvalues of the Jacobian of the chemical source terms. [6]. Among the existing approaches to the mixing timescale estimation [6], different studies demonstrated the capabilities of the so-called dynamic approach, based on the ratio of the scalar variance to the scalar dissipation rate. In this model, the scalar dissipation rate transport equation depends on a set of four constants, for which several different values are found in literature [6–8].

Despite the significant progresses in CFD calculations, their usage in real-life industrial scenarios is still very much limited to RANS simulations. Practical applications of LES, not to mention DNS, are still unfeasible in most situations because of their computational cost. In this context, a convenient pathway to meet the increasing industrial demand for affordable yet trustworthy predictions is to improve RANS reliability by quantifying the uncertainties associated with the numerical simulations. Turbulent combustion simulations are affected by several sources of uncertainty, which degrade the reliability of predictions [9, 10]: uncertainty in the system's geometry, boundary and initial conditions, as well as in numerical discretization and solution methods; uncertainty due to model form assumptions; parametric uncertainty due to lack of knowledge of model coefficients. We focus on the latter source of uncertainty. Uncertainty quantification (UQ) techniques were already employed to propagate uncertainties associated with chemical kinetics rate coefficients [11] and subfilter models' coefficients, e.g., Smagorinksy constant and turbulent Prandtl and Schmidt numbers [12] or spray dispersion models [13].

In this work, we investigate the predictive uncertainty of the PaSR combustion closure in RANS simulations due to the lack of knowledge of the scalar dissipation rate model parameters. We build Polynomial Chaos Expansions (PCE) surrogates [9, 14, 15] for the thermal flowfield in RANS simulations of the Cabra Flame in the methane/air configuration [1], as functions of the uncertain parameters. We exploit the PC surrogates to provide a global sensitivity analysis to such parameters and to drive the selection of a set of deterministically optimal parameters to recover experimental measurements.

2. Partially-stirred Reactor Model

At the core of the PaSR model is the assumption that the computational cell can be split into two locally uniform zones, one where reactions occur and one which is only characterized by mixing. The species concentration is determined by the mass exchange between the two zones. The mass fraction of the reactive region can be estimated as:

$$\kappa = \frac{\tau_c}{\tau_c + \tau_m} \tag{1}$$

where τ_c, τ_m are the characteristic chemical and mixing timescales, respectively. The mean source term in the species transport equation is then expressed as:

$$\widetilde{\dot{\omega}} = \kappa \frac{\bar{\rho}(Y_i^* - Y_i^0)}{\tau^*} \tag{2}$$

Y_i^0 is the initial i_{th} species mass fraction in the cell and Y_i^* is the i_{th} species mass fraction in the reactive region. To obtain Y_i^*, a time-splitting approach is employed: the reactive zone is modelled as a plug-flow reactor evolving from Y_i^0 over a residence time τ^*. In the present work, τ^* is chosen as the minimum between the mixing and the chemical timescale. While the chemical timescale is derived from the formation rates [3, 6], the mixing timescale is determined using the so-called dynamic approach:

$$\tau_{m_{dyn}} = \frac{\widetilde{Z^{"2}}}{\widetilde{\chi}} \tag{3}$$

where $Z^{"2}$ is the mixture fraction variance and χ is the scalar dissipation rate. The two scalars are modelled using the following transport equations [7]:

$$\frac{D\bar{\rho}\widetilde{Z^{"2}}}{Dt} = \frac{\partial}{\partial x_j}(\bar{\rho}(D + D_t))\frac{\partial Z^{"2}}{\partial x_j} + 2\bar{\rho}D_t(\frac{\partial \widetilde{Z^{"2}}}{\partial x_j})^2 - \bar{\rho}\widetilde{\chi} \tag{4}$$

$$\frac{D\bar{\rho}\widetilde{\chi}}{Dt} = \frac{\partial}{\partial x_j}(\bar{\rho}(D + D_t))\frac{\partial \chi}{\partial x_j} - C_{D1}\bar{\rho}\frac{\widetilde{\chi}^2}{\widetilde{Z^{"}2}} - C_{D2}\bar{\rho}\frac{\widetilde{\chi\epsilon}}{\widetilde{k}} + C_{P1}\frac{\widetilde{\chi}}{\widetilde{Z^{"}2}}P_f + C_{P2}\frac{\widetilde{\chi}}{\widetilde{k}}P_k \tag{5}$$

where Z is the mixture fraction, D and D_t are the molecular and turbulent diffusivity, $P_f = -2\bar{\rho}\widetilde{u_k^{"}Z^{"}}(\partial\widetilde{Z}/\partial x_k)$ is the production of scalar fluctuation and $P_k = -\bar{\rho}\widetilde{u_k^{"}u_i^{"}}(\partial\widetilde{U_i}/\partial x_k)$ is the production of turbulent kinetic energy.

Several values are proposed in literature for the coefficients $C_{P1}, C_{P2}, C_{D1}, C_{D2}$ [6–8]. These values were determined in quite different contexts, such as heat transfer in wall bounded turbulent flows, jet type flows, homogeneous flows behind a grid with a mean temperature gradient, premixed turbulent combustion and flameless combustion. To the authors' knowledge, no in-depth parametric study concerning the four constants exists in literature, as previous studies focused on a variety of test cases, ranging from lab-scale flames to semi-industrial furnaces, each of them only testing a few sets of constants.

In the present work, we systematically investigate and quantify the uncertainties in the thermal flow field prediction of a non-premixed lifted flame due to the lack of knowledge of the 4 scalar dissipation rate transport equation model parameters, that impact the determination of the mixing timescale in the dynamic PaSR closure. We employ Polynomial Chaos Expansions (PCEs) to efficiently describe the explicit functional relationships between uncertain inputs and output quantities of interest (QoIs), both represented as Random Variables (RVs).

3. Uncertainty Propagation

PCEs provide an approximate representation of random response functions in terms of finite-dimensional series expansions in standardized random variables [9, 14, 15]:

$$R(\boldsymbol{\xi}) \approx \sum_{i=0}^{P+1} \alpha_i \Psi_i(\boldsymbol{\xi}), \tag{6}$$

where α_i is a deterministic coefficient, Ψ_i is a multivariate functional built upon orthogonal polynomial basis sets, $\boldsymbol{\xi}$ is a vector, usually termed as *germ*, of random variables (i.e., model input variables) and $P+1$ is the number of terms at which the expansion is truncated. In this work, we consider all the random variables in $\boldsymbol{\xi}$ as normally distributed. Therefore, we employ Hermite orthogonal basis polynomials for the expansion and the multidimensional orthogonal polynomials $\Psi_i(\boldsymbol{\xi})$ in Eq. 6 are products of one-dimensional Hermite polynomials $\psi(\xi_k)$:

$$\Psi_i(\boldsymbol{\xi}) = \prod_{k=1}^{N} \psi_{t_k^i}(\xi_k). \tag{7}$$

In Eq. (7), N is the number of random variables, and the multi-index t_k^i represents an efficient way to encode the orders of each Hermite polynomial [15]. Here, a *total-order* expansion is employed, in which limits on the order of the polynomials are applied on the sum of the Hermite polynomials order, which compose the functionals in equ. 7. Namely, the expansion term multi-index t_k^i defining the set of Ψ_i is constrained by $sum_k t_k^i \leq p_i$, where p_i is the polynomial order bound for the i-th dimension. The tensor-product expansion therefore allows polynomial order bounds to be specified independently for each dimension. We evaluate the polynomial coefficients α_i in Eq. (6) using spectral projections of R against the subspace spanned by each functional Ψ_i, according to the following equation:

$$\alpha_i = \frac{\langle R_\xi, \Psi_i \rangle}{\langle \Psi_i^2 \rangle} = \frac{1}{\langle \Psi_i^2 \rangle} \int_\Omega R_\xi \, \Psi_i \rho_x(\boldsymbol{\xi}) d\boldsymbol{\xi}, \tag{8}$$

where $\langle . \rangle$ denotes the inner product, ρ_x is the input parameters' multivariate normal probability density function. Simulation methods, e.g., random sampling, or deterministic approaches, e.g. cubature methods, can be used to evaluate the 4-dimensional integral in Eq. (8). Both methods rely on a set of deterministic model resolutions, corresponding to some specific realizations of $\boldsymbol{\xi}$, thus belonging to the class of *non-intrusive* PCE methods. Given the cost of a model realization, i.e., one RANS computation, the not too large dimensionality of the integral, and the slow convergence rate of sampling methods, we approximate the integral with a 4-dimensional tensor-product cubature rule:

$$\alpha_i \approx \frac{1}{\langle \Psi_i^2 \rangle} \sum_{j=1}^{N_c} R(\boldsymbol{\xi}^{(j)}) W^{(j)}, \tag{9}$$

where N_c represents the number of cubature nodes, RANS solutions of the thermal flow field in given spatial locations are used to extract R over the corresponding node $\boldsymbol{\xi}^{(j)}$, and $W^{(j)}$ are the weights of the rule in each node. To alleviate the curse of dimensionality of such rules, hence reducing the number of cubature nodes, we resort to sparse grid tensorization. Sparse grids were proposed by Smolyak [16] for use in high-dimensional problems to provide similar accuracy as full tensor-product expansions, while requiring significantly fewer collocation points, as shown in several studies where sparse grids were used [17–21]. The sparse grid method is computationally efficient for moderately high-dimensional problems. It uses linear combinations of carefully selected tensor products to preserve the interpolation property for a high-dimensional random space [20].

In this work, we employ a sparse grid with level l=2 and Genz-Keister rules to evaluate the spectral projections and map the uncertain parameters to the predicted profiles of temperature in the investigated flame. Once obtained, the meta-model $R(\boldsymbol{\xi})$ in Eq. (6) will be used to perform a global sensitivity analysis at no cost. Interactions between different parameters are accounted for, as well as non linear effects on model responses. The fractional contribution of each random input to the overall model predictive uncertainty can be estimated via the *main-effect* Sobol

indices [22, 23]:

$$S_k = \frac{V_{\xi_k}(E_{\xi_{\sim k}}(R(\boldsymbol{\xi})|\xi_k))}{V(R(\boldsymbol{\xi}))} = \frac{\sum_{k=1}^{L}\alpha_i^2}{\sum_{i=1}^{P+1}\alpha_j^2} \quad (10)$$

where $V(R(\boldsymbol{\xi}))$ is the total variance of the model response, and the numerator represents the variance determined by the k-th variable, calculated with respect to an expected value of the model response. The latter is obtained by varying all the random variables within their full uncertainty ranges, but the k-th one ($\xi_{\sim k}$), kept constant. As suggested in Eq. (10), the GSA indices are related to the functional coefficients in Eq. (6). In Eq. (10), L is the number of expansion terms containing only Hermite polynomials of nonzero order for the k-th variable. The contribution to the output variance of ξ_k, including the variance caused by its interactions with the other input variables, is computed with the *total-effect* indices:

$$S_{T_k} = 1 - \frac{V_{\xi_{\sim k}}(E_{\xi_k}(R(\boldsymbol{\xi}|\xi_{\sim k}))}{V(R(\boldsymbol{\xi}))} \quad (11)$$

4. Application

4.1. RANS of the Cabra flame

The test case used in the present work is the methane-air Cabra flame described in [1]. This vitiated coflow flame consists of a lifted jet flame formed by a fuel jet issuing from a central nozzle into a coaxial flow of hot combustion products from a premixed hydrogen/air flame. The numerical domain consists of a structured 2D axisymmetric grid of 30000 cells; Fig. 1 shows a sketch of the flame setup. A grid convergence study can be found in the supplemental material. The uRANS simulations are carried out using the FiReSMOKE solver [24], based on the OpenFOAM®framework. Turbulence is modelled using

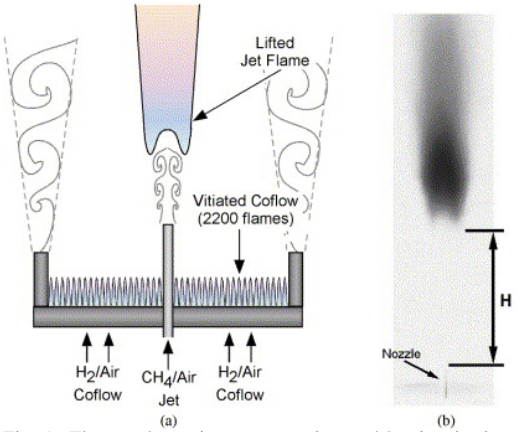

Fig. 1: Flame schematic representation and luminosity image of the methane-air Cabra flame. Adapted from [1].

the $k-\varepsilon$ model with Pope's correction for round jets [25]. The PaSR model examined in Sec. 2 is employed to handle the turbulence-chemistry interaction. The 57 species, 268 reactions kinetic mechanism from San Diego [26] is employed for all simulations, based on a preliminary investigation on the sensitivity to the kinetic mechanism. These results can be found in the supplementary material along with preliminary simulations which explain the choice of turbulence model and using different formulations of the mixing timescale discussed in the previous section to assess the potential gain associated to a dynamic formulation of τ_m (Eq. 3).

4.2. Uncertain Parameters Definition

The explicit probability distributions of the uncertain model coefficients are required to build the input parameters' space and consequently determine the cubature nodes. The values of the 4 coefficients in Eq.(5) employed in several literature studies [6–8] are shown in Table 1. We assign a normal distribution to each of the uncertain parameters and we use such values to define their mean $\bar{C}_i$ and standard deviations σ_i, which are shown in Table 2. Note that the values for C_{P2} show very little variance compared to the other three.

	C_{P1}	C_{P2}	C_{D1}	C_{D2}
Jones-Musonge [7]	1.7	1.45	1	0.9
Borghi [7]	0.5	1	1.9	0.95
Mantel-Borghi [7]	1	1.45	0.625	0
Chen [7]	0.5	1.45	1.15	0.65
Ferrarotti C1 [8]	0.85	1.45	2	0.9
Ferrarotti C2 [8]	1.7	1.45	2	0.9
Li 1 [6]	1.7	1.4	2	1.8
Li 2 [6]	1.7	1.4	1	1.8
Ye 1 [27]	0.85	1.4	2	1.8
Ye 2 [27]	1.7	1.4	1	1.8
Ye 3 [27]	1.7	1.4	2	1.8
Ye 4 [27]	0.85	1.4	1	1.8

Table 1: Literature constants sets used to determine the 4D parameter space for the UQ analysis. Values taken from [6–8, 27].

Henceforth, as mentioned in section 3, the sampled input parameters for each simulation are determined using a 4-dimensional nested sparse grid of level 2. This results in a total of 57 simulations required to evaluate the coefficients α_i as per Eq.(9) up to second-order (P=14 in Eq.(7)) and carry out the UQ analysis.

	C_{P1}	C_{P2}	C_{D1}	C_{D2}
C_i	1.229	1.388	1.473	1.258
σ_i	0.205	0.050	0.219	0.247

Table 2: Mean and standard deviation for the four input parameters.

5. Results

The evaluation of the PCE coefficients allows the reconstruction of closed-form polynomial expressions of the QoIs probability distributions as functions of the uncertain input parameters. Once these distributions are known, crucial information about the reliability of RANS simulations predictions become available. Random sampling from such distributions enables the computation of statistics, e.g. median, variance, and percentiles. Note that the cost of one evaluation of the surrogate model is negligible. The output QoIs considered for this analysis are the Favre-averaged temperature T and mixture fraction Z, being the ability to appropriately capture the lift-off height the key point in simulating this burner configuration. Experimental measurements are available [1] for direct comparison of the uncertainty intervals.

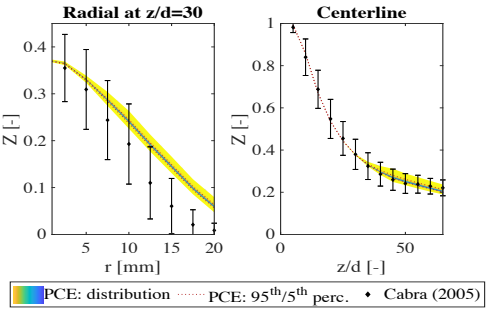

Fig. 2: Radial and axial profiles of favre-averaged mixture fraction PDFs. Red dots indicate 95^{th}/5^{th} percentiles. Black dots and bars represent experimental values and their measured RMS.

5.1. Uncertainty Propagation

The uncertainty in the evolution of the mixture fraction are shown in Fig. 2 on the centerline and on a radial profile at a selected distance from the inflow ($z/D = 30$). Close to the nozzle, where only mixing occurs, the uncertainty band is narrow, i.e., the mixture fraction is predicted with very high confidence. Starting from $z/D = 30$ the uncertainty increases, especially close to the centerline. This is due to the increase in both the mixture fraction variance and scalar dissipation rate that occurs as the flame ignites. The maximum relative distance between the 95^{th}/5^{th} percentiles curves and the median is 7.8%/3.6%.

The predictive uncertainty bands of temperature due to the uncertain model parameters are shown in Fig. 3. By observing the narrow uncertainty at the first radial position ($z/D = 15$) and along the centerline up to $z/D \approx 30$, we infer that the impact of the investigated model parameters in the regions where only mixing occurs and the flame is not yet ignited is negligible. From the experimental data collected and from visual investigation, Cabra et al. [1] established the liftoff height near $z/D = 35$. As a matter of fact, an increase in the experimental temperature fluctuations is observed at $z/D = 40$ along with an increase of the mean temperature above the coflow inlet value. On the other hand, the PaSR model slightly underpredicts the liftoff height, as we can observe a definite increase in the predicted temperature profile starting from $z/D = 30$. The liftoff prediction result is in line with previous works, which employed flamelet-based models [28] and the more computationally expensive transported PDF models [1, 29, 30], while PaSR simulations yield a better prediction of the temperature profiles in the positions considered. As chemical reactions begin to occur, temperature uncertainty becomes significant. As expected, model predictions are less confident at higher temperature, given the influence the scalar dissipation rate holds on the mixing time and species average source term integration time. Looking at the radial profiles in Fig. 3, the highest variability from the predicted median value can be found at $z/D = 30, 40$ and 50, where the maximum temperature for the 95^{th}/5^{th} percentiles is respectively 7.0%/4.5% of the median maximum temperature. It is interesting to note that the experimental measurements RMS and the probability bands have opposite trends at $z/D = 70$: while the measured temperature fluctuations grow larger at the outer edge of the radial profile, the predicted uncertainty band narrows. This can be explained by the fact that the experimental values fluctuations are due to the mixing with the outer air stream (measured temperatures drop below the coflow inlet value) that starts to affect the flame in the downstream region. However, this is not affecting our current numerical simulations, as the outer stream is not included in the numerical model. Along the centerline, the uncertainty band steadily grows larger as the temperature increases, starting from $z/D \approx 40$. The maximum spread between the 95^{th}/5^{th} percentiles curves and the median temperature is 5.9%/4.6%.

5.2. Sensitivity Analysis

The PC surrogate model allows us to perform a global sensitivity analysis in order to determine the impact each one of the four parameters has on the uncertainty in the QoIs. Figure 4 shows the main and total effect sensitivity indices for the Favre-averaged temperature at the $z/D = 30$ location and along the centerline of the flame, starting from $z/D = 30$. As mentioned in section 3, these indices are normalized with respect to the total variance of the model response for the selected QoI. Focusing on the main effect (i.e. the indices calculated using only the first-order coefficients) one can see how most of the uncertainty is due to the two dissipation constants C_{D1} and C_{D2}, with the second one being more important as the predicted temperature increases. This result can be explained considering that the C_{D1} and C_{D2} are the parameters relative to the dissipation of scalar fluctuations and turbulent kinetic energy, respectively. The scalar

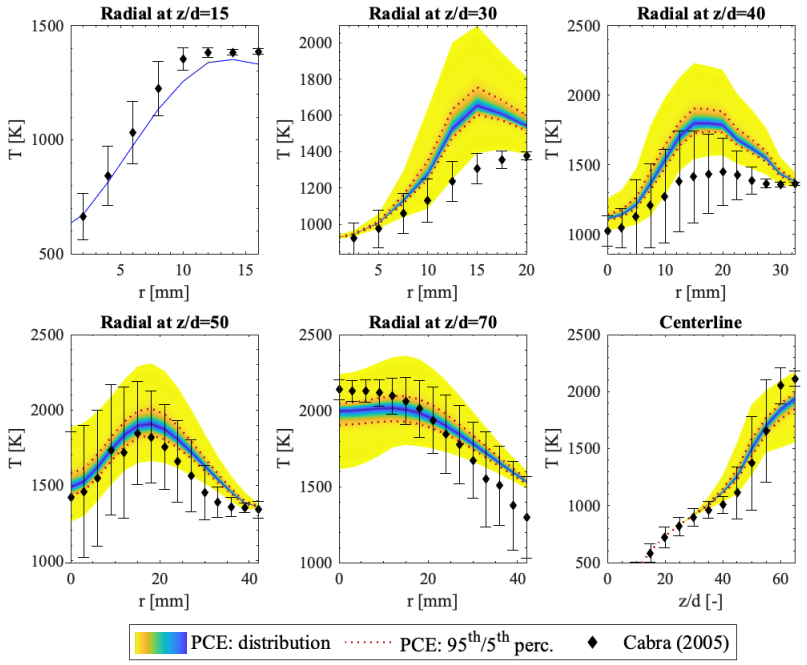

Fig. 3: Radial and axial profiles of favre-averaged temperature PDFs. Red dots indicate $95^{th}/5^{th}$ percentiles. Black dots and bars represent experimental values and their measured RMS.

dissipation fluctuations are in fact most prominent in the ignition and extinction regions and this behaviour is reflected in the fractional contribution to the uncertainty associated to the parameter C_{P1}. On the other hand the sensitivity indices for the two production parameters C_{P1} and C_{P2} hold less influence over the global uncertainty, with the latter having virtually no effect in the downstream regions and farther from the centerline.

This behaviour strongly changes if we look at the total effect indices, determined by also including second-order terms in their calculation. The most significant change can be found in the sensitivity to the C_{P1} parameter. Contrary to the main effect analysis, the first production parameter holds a constant value across both the radial and centerline profiles. To a lesser degree, the global uncertainty sensitivity to C_{P2} also increases across the board. The total effect analysis then shows that second order effects and the cross-coupling between the parameters have a definite effect on the overall uncertainty of the QoI which must be taken into account.

The sensitivity analysis confirms a trend that was already inferred in literature [3, 6, 8], as C_{D1} and C_{D2} were already found to have the largest influence on the predicted temperature profiles. However, our analysis adds to these empirical findings a quantitative support. An accurate determination of the uncertainty related to the scalar dissipation rate modelling can indeed lead to improvements in the mixing modelling which is one of the most critical links in many combustion closures such as transported probability density function approach.

5.3. Deterministic Optimization

Lastly, the surrogate models $R(\boldsymbol{\xi})$ are employed in an exhaustive search to find the optimal set of coefficients as:

$$\underset{\boldsymbol{\xi}}{\operatorname{argmin}} \left(\frac{1}{N_{exp}} \sum_{j}^{N_{exp}} \frac{(e_j - R_j(\boldsymbol{\xi}))^2}{(3\sigma(e_j))^2} \right) \qquad (12)$$

where e_j are the experimental values, $\sigma(e_j)$ is the experimental standard deviation, N_{exp} is the number of experimental points. The resulting parameter combination is reported in Table 3. Figure 5 shows

	C_{P1}	C_{P2}	C_{D1}	C_{D2}
Opt	1.6053	1.1978	1.5604	1.1854

Table 3: Optimal set of parameter determined from minimizing Eq.(12).

the predicted temperature profiles, against experimental measurements and the numerical simulation obtained with the coefficients named Li-2 in Table 1, already employed in [6]. While the lift-off height is still slightly underpredicted at $z/D = 30$, the results mostly fall within the experimental uncertainties in the remaining axial positions and improve the predictions obtained with the Li-2 set of coefficients.

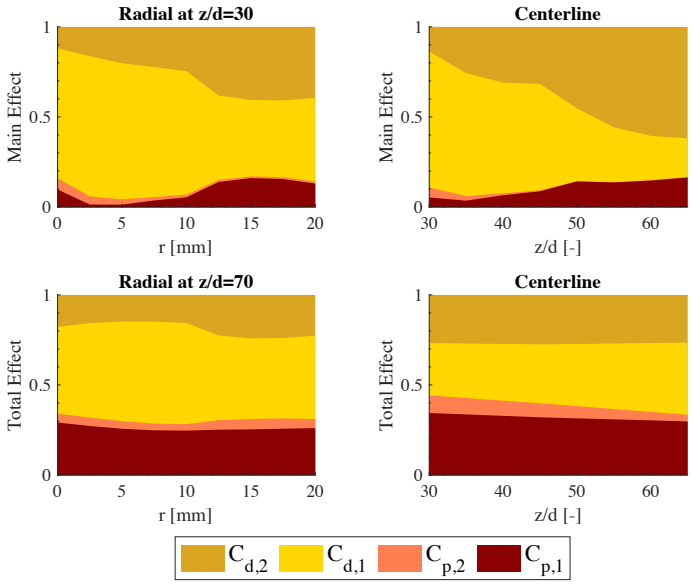

Fig. 4: Main and total effect sensitivity indices for the favre-averaged temperature at $z/D = 70$ and centerline.

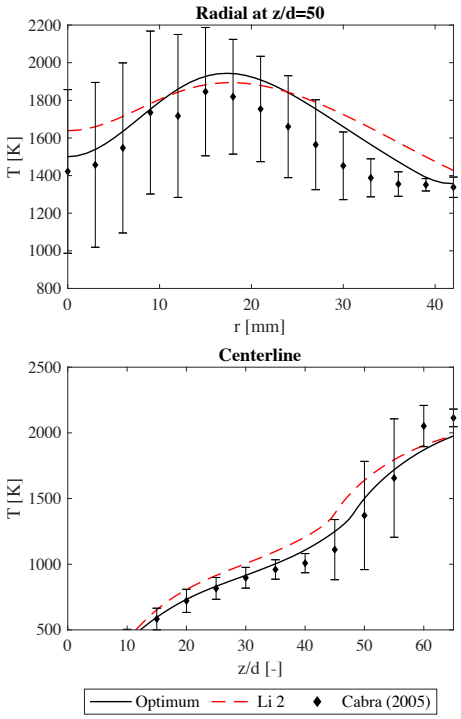

Fig. 5: Radial $z/D = 50$ and centerline predicted temperature profile obtained with the optimum set of parameters (black), with the *Li 2* set (red), and experimental measurements (black diamonds) with their RMS.

6. Conclusions

An uncertainty quantification study for Reynolds-Averaged Navier-Stokes simulations of the methane-fed Cabra flame is presented. Polynomial Chaos Expansions are employed to build surrogate models to efficiently assess the effect of parametric uncertainty in the four parameters of the scalar dissipation rate transport equation used in the context of the dynamic Partially-Stirred Reactor combustion model. The PCE coefficients are obtained with sparse grid cubature using Genz-Keister rules. The uncertainty is then propagated to the predictions of mixture fraction and temperature. The results show the effectiveness of the approach to provide predictions with estimates of uncertainty. The highest uncertainty is found as temperature increases, because of the influence of the scalar dissipation rate holds on the mixing timescale determination. The surrogate models are then employed to perform a variance-based sensitivity analysis of the four parameters of the model. Analyzing both first and second order effects on the output variance, it is found that the two dissipation coefficients C_{D1}, C_{D2} hold the strongest influence on the variability of the model response across all regions of the flame. Second order effect analysis shows that cross correlation effects between the parameters must not be neglected. Finally, an optimization procedure using experimental results as targets is followed to determine an optimal set of parameters. The resulting set of constants yields improved predictions of both mixture fraction and temperature. Future developments will focus on the extension of this UQ approach to model form and model parameter uncertainties associated with turbulence and chemical kinetics modelling, in the perspective of providing a more comprehensive quantification of uncertainty in RANS modelling of turbulent flames.

Acknowledgments

This publication benefits from the support of the Walloon Region as part of a FRIA grant funding. This project has also received funding from the European

Research Council (ERC) under the European Union's Horizon 2020 research and innovation program under grant agreement No. 714605 and Marie Skłodowska-Curie grant agreement No 801505.

Supplementary material

Additional analysis and data mentioned in the paper is available in the supplementary material.

References

[1] R. Cabra, J.-Y. Chen, R. Dibble, A. Karpetis, R. Barlow, Lifted methane–air jet flames in a vitiated coflow, Combustion and Flame 143 (4) (2005) 491–506, special Issue to Honor Professor Robert W. Bilger on the Occasion of His Seventieth Birthday.

[2] A. Parente, C. Galletti, L. Tognotti, Effect of the combustion model and kinetic mechanism on the mild combustion in an industrial burner fed with hydrogen enriched fuels, International Journal of Hydrogen Energy 33 (24) (2008) 7553–7564.

[3] M. Ferrarotti, Z. Li, A. Parente, On the role of mixing models in the simulation of mild combustion using finite-rate chemistry combustion models, Proceedings of the Combustion Institute 37 (4) (2019) 4531–4538.

[4] R. Cabra, T. Myhrvold, J. Chen, R. Dibble, A. Karpetis, R. Barlow, Simultaneous laser raman-rayleigh-lif measurements and numerical modeling results of a lifted turbulent h2/n2 jet flame in a vitiated coflow, Proceedings of the Combustion Institute 29 (2) (2002) 1881–1888.

[5] J. Chomiak, Combustion A Study in theory, fact and application, 1990.

[6] Z. Li, M. Ferrarotti, A. Cuoci, A. Parente, Finite-rate chemistry modelling of non-conventional combustion regimes using a partially-stirred reactor closure: Combustion model formulation and implementation details, Applied Energy 225 (2018) 637–655.

[7] J. P. H. Sanders, I. Gökalp, Scalar dissipation rate modelling in variable density turbulent axisymmetric jets and diffusion flames, Physics of Fluids 10 (4) (1998) 938–948.

[8] M. Ferrarotti, M. Fürst, E. Cresci, W. de Paepe, A. Parente, Key modeling aspects in the simulation of a quasi-industrial 20 kw moderate or intense low-oxygen dilution combustion chamber, Energy & Fuels 32 (10) (2018) 10228–10241.

[9] O. Le Maître, O. M. Knio, Spectral methods for uncertainty quantification: with applications to computational fluid dynamics, Springer Science & Business Media, 2010.

[10] V. Raman, M. Hassanaly, Emerging trends in numerical simulations of combustion systems, Proceedings of the Combustion Institute 37 (2) (2019) 2073–2089.

[11] D. A. Sheen, H. Wang, The method of uncertainty quantification and minimization using polynomial chaos expansions, Combustion and Flame 158 (12) (2011) 2358–2374.

[12] M. Khalil, G. Lacaze, J. C. Oefelein, H. N. Najm, Uncertainty quantification in les of a turbulent bluff-body stabilized flame, Proceedings of the Combustion Institute 35 (2) (2015) 1147–1156.

[13] P. P. Ciottoli, A. Petrocchi, L. Angelilli, F. E. H. Perez, R. M. Galassi, F. Picano, M. Valorani, H. G. Im, Uncertainty Quantification Analysis of RANS of Spray Jets.

[14] N. Wiener, The homogeneous chaos, American Journal of Mathematics 60 (4) (1938) 897–936.

[15] R. G. Ghanem, P. D. Spanos, Stochastic Finite Elements: A Spectral Approach, Springer, New York, NY, 1990.

[16] S. Smolyak, Quadrature and interpolation formulas for tensor products of certain classes of functions, Doklady Akademii Nauk SSSR 148 (1963) 1042–1045.

[17] T. Gerstner, M. Griebel, Numerical integration using sparse grids, Numerical Algorithms 18 (3-4) (1998) 209–232.

[18] F. Nobile, R. Tempone, C. G. Webster, A sparse grid stochastic collocation method for partial differential equations with random input data, SIAM Journal on Numerical Analysis 46 (5) (2008) 2309–2345.

[19] M. Eldred, J. Burkardt, Comparison of Non-Intrusive Polynomial Chaos and Stochastic Collocation Methods for Uncertainty Quantification, 2009, Ch. Paper 2009–0976, pp. 1–20.

[20] K. Judd, L. Maliar, S. Maliar, R. Valero, Smolyak method for solving dynamic economic models: Lagrange interpolation, anisotropic grid and adaptive domain, Journal of Economic Dynamics and Control 44 (2014) 92–123.

[21] J. Son, Y. Du, Comparison of intrusive and nonintrusive polynomial chaos expansion-based approaches for high dimensional parametric uncertainty quantification and propagation, Computers & Chemical Engineering 134 (2020) 106685.

[22] I. Sobol', Global sensitivity indices for nonlinear mathematical models and their monte carlo estimates, Mathematics and Computers in Simulation 55 (1) (2001) 271–280, the Second IMACS Seminar on Monte Carlo Methods.

[23] T. Ziehn, A. S. Tomlin, A global sensitivity study of sulfur chemistry in a premixed methane flame model using hdmr, International Journal of Chemical Kinetics 40 (11) 742–753.

[24] FiReSMOKE, a collection of finite-rate chemistry solvers for combustion simulations for openfoam.
URL https://github.com/burn-research/FiReSMOKE

[25] S. B. Pope, An explanation of the turbulent round-jet/plane-jet anomaly, AIAA Journal 16 (3) (1978) 279–281.

[26] San Diego Mechanism web page, Mechanical and Aerospace Engineering (Combustion Research), UCSD, Chemical-Kinetic Mechanisms for Combustion Applications (2021).
URL https://web.eng.ucsd.edu/mae/groups/combustion/mechanism.html

[27] I. K. Ye, Investigation of the scalar variance and scalar dissipation rate in urans and les, Ph.D. thesis, University of Waterloo (2011).

[28] J.-B. Michel, O. Colin, C. Angelberger, D. Veynante, Using the tabulated diffusion flamelet model adf-pcm to simulate a lifted methane–air jet flame, Combustion and Flame 156 (7) (2009) 1318–1331.

[29] R. L. Gordon, A. R. Masri, S. B. Pope, G. M. Goldin, Transport budgets in turbulent lifted flames of methane autoigniting in a vitiated co-flow, Combustion and Flame 151 (3) (2007) 495–511.

[30] K. Gkagkas, R. Lindstedt, Transported pdf modelling with detailed chemistry of pre- and auto-ignition in ch4/air mixtures, Proceedings of the Combustion Institute 31 (1) (2007) 1559–1566.